Superficial white matter fiber systems impede detection of long-range cortical connections in diffusion MR tractography

Colin Reveley[a], Anil K. Seth[a], Carlo Pierpaoli[b], Afonso C. Silva[c], David Yu[d], Richard C. Saunders[e], David A. Leopold[d,e,1], and Frank Q. Ye[d]

[a]Sackler Center for Consciousness Science, School of Engineering and Informatics, University of Sussex, Brighton BN1 9QJ, United Kingdom; [b]Program on Pediatric Imaging and Tissue Sciences, Eunice Kennedy Shriver National Institute of Child Health and Human Development, National Institutes of Health, Bethesda, MD 20892; [c]Cerebral Microcirculation Section, Laboratory of Functional and Molecular Imaging, National Institute of Neurological Disorders and Stroke, National Institutes of Health, Bethesda, MD 20892; [d]Neurophysiology Imaging Facility, National Institute of Mental Health, National Institute of Neurological Disorders and Stroke, and National Eye Institute, National Institutes of Health, Bethesda, MD 20892; and [e]Laboratory of Neuropsychology, National Institute of Mental Health, National Institutes of Health, Bethesda, MD 20892

Edited by Peter L. Strick, University of Pittsburgh, Pittsburgh, PA, and approved April 22, 2015 (received for review September 20, 2014)

In vivo tractography based on diffusion magnetic resonance imaging (dMRI) has opened new doors to study structure–function relationships in the human brain. Initially developed to map the trajectory of major white matter tracts, dMRI is used increasingly to infer long-range anatomical connections of the cortex. Because axonal projections originate and terminate in the gray matter but travel mainly through the deep white matter, the success of tractography hinges on the capacity to follow fibers across this transition. Here we demonstrate that the complex arrangement of white matter fibers residing just under the cortical sheet poses severe challenges for long-range tractography over roughly half of the brain. We investigate this issue by comparing dMRI from very-high-resolution ex vivo macaque brain specimens with histological analysis of the same tissue. Using probabilistic tracking from pure gray and white matter seeds, we found that ∼50% of the cortical surface was effectively inaccessible for long-range diffusion tracking because of dense white matter zones just beneath the infragranular layers of the cortex. Analysis of the corresponding myelin-stained sections revealed that these zones colocalized with dense and uniform sheets of axons running mostly parallel to the cortical surface, most often in sulcal regions but also in many gyral crowns. Tracer injection into the sulcal cortex demonstrated that at least some axonal fibers pass directly through these fiber systems. Current and future high-resolution dMRI studies of the human brain will need to develop methods to overcome the challenges posed by superficial white matter systems to determine long-range anatomical connections accurately.

diffusion MRI | tractography | neuroanatomy | white matter | connectome

The primate cerebral cortex consists of dozens of areas distinguished by their cytoarchitectonic profiles (1), sensory maps (2), functional specialization (3), and spontaneous activity covariation (4). Attention within neuroscience has increasingly focused on understanding how connectivity among these regions underpins brain function in health and in disease (5). The macaque monkey (*Macaca mulatta*) has been a fruitful neuroscientific model because the functional organization of its brain is similar in many ways to that of the human (6–8). Tracer injections in the macaque have revealed that virtually all cortical areas give rise to long-range connections, many of which project to other cortical areas, potentially to form processing hierarchies (9). This understanding continues to shape views of functional organization in the human brain. However, studying long-range connections through tracer injections is time consuming, inefficient, and prone to sampling biases, because a given experiment can measure connectivity to only one or a small number of cortical sites. Moreover, although in many respects the macaque brain is a good approximation of the human brain, both species have undergone profound evolutionary changes since the time of their most recent common ancestor living more than 20 million years ago (10), particularly in regard to the massive expansion of the cerebral cortex in the human brain (11). Thus, it is of great value to assess human anatomical connections directly and comprehensively (12), a recognition that is central to the Human Connectome Project (13, 14).

Studying human neuroanatomical connections poses distinct experimental challenges, because tract tracing must be conducted either noninvasively or postmortem (5). Postmortem tracer studies, e.g., using carbocyanine dyes (15, 16), allow some tracking of corticocortical connections. However, questions about the accuracy of these methods in the adult brain have limited their use (17, but see ref. 18). MRI is the more common method used to evaluate neuroanatomical connections in the human brain and has the advantage of being noninvasive and applicable to live subjects, including patients (19). Foremost among MRI methods for inferring long-range anatomical connections is diffusion-weighted MRI, often abbreviated as "diffusion MRI" or simply "dMRI." In dMRI, the local anisotropic diffusion profile of water molecules within each voxel is taken as a basis for inferring the local fiber orientation distribution, in the simplest case described as a tensor model with a single principal

Significance

It is widely recognized that studying the detailed anatomy of the human brain is of great importance for neuroscience and medicine. The principal means for achieving this goal is presently diffusion magnetic resonance imaging (dMRI) tractography, which uses the local diffusion of water throughout the brain to estimate the course of long-range anatomical projections. Such projections connect gray matter regions through axons that travel in the deep white matter. The present study combines dMRI tractography with histological analysis to investigate where in the brain this method succeeds and fails. We conclude that certain superficial white matter systems pose challenges for measuring cortical connections that must be overcome for accurate determination of detailed neuroanatomy in humans.

Author contributions: C.R., A.K.S., C.P., A.C.S., D.A.L., and F.Q.Y. designed research; C.R. and F.Q.Y. performed research; A.C.S., D.Y., R.C.S., and F.Q.Y. contributed new reagents/analytic tools; C.R., D.Y., R.C.S., and F.Q.Y. analyzed data; and C.R., A.K.S., C.P., A.C.S., D.A.L., and F.Q.Y. wrote the paper.

The authors declare no conflict of interest.

This article is a PNAS Direct Submission.

Freely available online through the PNAS open access option.

[1]To whom correspondence should be addressed. Email: LeopoldD@mail.nih.gov.

This article contains supporting information online at www.pnas.org/lookup/suppl/doi:10.1073/pnas.1418198112/-/DCSupplemental.

www.pnas.org/cgi/doi/10.1073/pnas.1418198112

axis (20, 21). A range of diffusion models and algorithms has been developed over the past two decades in an attempt to derive anatomical pathways from features of the water diffusion displacement profile in each voxel. These methods, generally termed "dMRI tractography" (22–25), can be divided into deterministic methods, in which the best estimates of various pathways are depicted as streamlines or streamtubes, and probabilistic methods, in which a family of possible trajectories is estimated accounting for noise-induced uncertainty.

dMRI methods have proven remarkably successful in the modeling of large white matter bundles in vivo in human volunteers (26). Although there are certain inherent challenges, such as the difficulty in following the course of fiber tracts through regions consisting of crossing or abutting fiber pathways, these problems have been ameliorated by improvements in both local orientation modeling and tractography algorithms (27). At present, the most successful fiber tracking employs probabilistic or deterministic approaches on high-angular-resolution diffusion imaging (HARDI) or diffusion spectrum imaging data. Comparison with known fiber pathways has been used to validate computed dMRI track lines at a qualitative level (28), and studies in animals have compared diffusion methods to the results from anatomical tracer experiments, sometimes in the same brains (29–31). In recent years the clinical value of this method has become apparent, as tractography has become a viable tool both for surgical planning (32) and the monitoring of neuropathology (33).

Building on these successes, many investigators now use diffusion tractography to identify and study long-range projections of the cerebral cortex, including corticocortical projections. The neurons that compose these projections send their axons from cell bodies in the gray matter into fasciculi in the deep white matter. After traveling through the deep white matter, the axons emerge to enter a different cortical region. Thus, the use of dMRI to track corticocortical connections involves two additional and daunting challenges. The first challenge is that the diffusion anisotropy measured in the cortex and near the white matter/gray matter boundary (WGB) often is too low to model local orientation, which is a prerequisite for inclusion in a track line. The second challenge is that it is extremely difficult to determine precisely where small axonal tracts join and leave larger white matter fasciculi (34). These limitations have prompted neuroscientists to adopt pragmatic heuristics for studying cortical connectivity using dMRI. For example, to facilitate the crossing of the WGB, it has become common practice to construct large-volume cortical seeds that include a portion of the adjacent white matter, just deep to the infragranular layers of cortical neurons. Then, to combat the inherently ambiguous detection of axonal branching in deep white matter fasciculi, investigators often apply "waypoints," which create a priori spatial restrictions that selectively limit the results to fibers along trajectories of interest. Although debatable at a theoretical level, these methods allow investigators to visualize certain types of corticocortical connections that otherwise would resist characterization by the dMRI method. A common assumption is that in the future, when the spatial and angular resolution of dMRI acquisition improves, fewer such methodological adjustments will be required to obtain accurate results.

A recent study comparing tract-tracer and dMRI tractography concluded that the anatomical accuracy of dMRI tractography is intrinsically limited, but it did not investigate the specific factors leading to this finding (35). In the present study, we investigate the viability of tractography at high resolution, addressing the critical question of whether projections could be followed accurately between the cortex and deep white matter. We obtained and analyzed dMRI datasets of exceptional quality from ex vivo rhesus macaque brains and compared tracking successes and failures with local histological features on myelin-stained sections of the subsequently processed brains. We focused on intrinsic white matter features in the vicinity of the WGB and their impact on the accurate detection of long-range cortical connections. We first demonstrate that, in agreement with previous findings (36–38), tractography methods are biased in their identification of long-range projections toward cortical gyri. Based on detailed examination of both the dMRI data and accompanying histological sections, we next determine that much of this bias can be ascribed to the challenges associated with the complex arrangement of superficial white matter fiber systems commonly known as "local association fibers" (39, 40). These intrinsic systems impede tractography by acting as barriers that prevent communication of track lines between the cortex and deeper white matter, even when HARDI modeling is used. Crucially, ~50% of cortical locations were affected by such white matter barriers, thus strongly limiting the detectability of cortical connections throughout the brain using current methods. Because long-range cortical projections begin and terminate in the gray matter, the capacity of dMRI methods to negotiate the WGB is of great importance. Thus, the navigation through superficial white matter systems is a significant challenge that will need to be overcome for diffusion methods to provide a more accurate portrait of anatomical connections in the human brain.

Results

Tractography and histological analysis were performed on the fixed brains of two rhesus macaque monkeys. The dMRI datasets were obtained ex vivo on a 7-T horizontal Bruker scanner, with each brain specimen scanned over a period exceeding 61 h (*Methods*). Data from one of the brains were used in our previously published study (35). The resulting dMRI data had an isotropic spatial resolution of 250 μm and a diffusion orientation resolution of 60 or 126 directions. With the ex vivo scanning approach, we were able to minimize the contribution of factors that adversely affect human tractography, such as partial-volume effects, subject motion and physiological fluctuations, and poor signal-to-noise ratio (SNR). Following scan acquisition, the tissue was processed for histological analysis. Myelin-stained sections were registered subsequently with the dMRI data from the same monkey, allowing us to compare tractography results directly with the course of visible axonal fibers and other anatomical features.

An example of a local dMRI data slice and corresponding histological sections from the same brain are shown in Fig. 1, which features a region in and near the rostral opening of the intraparietal sulcus (IPS). The maps in Fig. 1 *B–D* show the local 3D diffusion orientation as colored line segments superimposed on a gray-scale map of fractional anisotropy (FA). The cyan curve is an estimation of the WGB determined using a separate magnetization transfer (MT) contrast MRI scan (*Methods*). The high SNR of the acquisition made it possible to determine at least one, and often more than one, diffusion orientation throughout the gray matter despite its low overall FA (Figs. S1 and S2). Across the brain, the principal diffusion orientation in the cortex nearly always was perpendicular to the WGB, with the exception of the deepest cortical layers in some regions. This regularity was in sharp contrast to the principal diffusion orientation in the superficial white matter, operationally defined here as a zone deep to the infragranular cell layers of the cortex and within 1 mm from the WGB (corresponding to fewer than four voxels in the current datasets). The principal orientation of the computed diffusion direction in this superficial white matter orientation varied widely relative to the overlying WGB plane and thus relative to the diffusion orientation of the overlying cortex. This range of relative diffusion orientations is exemplified in the red and green regions magnified in Fig. 1 *C* and *D*. The principal fiber orientation in the magnified green region, from the gyral crown of the inferior parietal lobule (IPL), is nearly perpendicular to the WGB and hence is

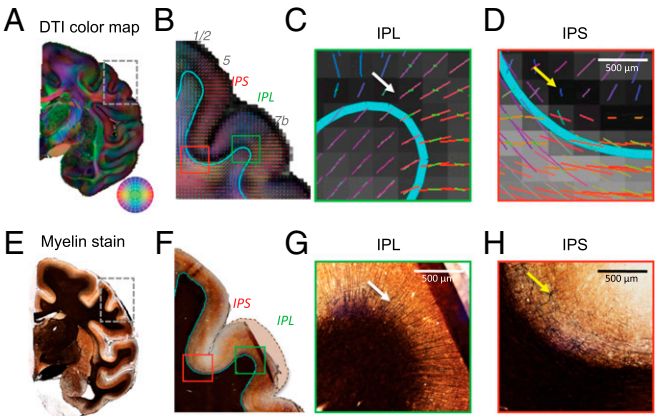

Fig. 1. Examples of diffusion MRI and histological datasets used in this study. (*A*) dMRI data collected at 250-μm isotropic resolution showing a coronal slice colored by dominant direction [diffusion tensor imaging (DTI) principal eigenvector]. Direction is shown in the color wheel on the lower right. (*B*) The *Inset* in *A*, focusing on a region in and around the IPS and IPL. The colored lines in each voxel correspond to the FSL crossing fiber mean model orientation, colored as in *A*. The lines are overlaid on a map of FA derived from DTI analysis. The cyan contour is the WGB derived from the MT contrast and surface reconstruction (*Methods*). (*C* and *D*) The green (*C*) and red (*D*) boxed areas in *B* showing subregions of the IPL and IPS at greater magnification. (*C*) Magnified region of the IPL showing the orderly trajectory of principal orientations flowing from the white matter into the IPL. The white arrow indicates the highly oriented model fibers within the cortical gray matter. (*D*) Magnified region of the IPS in which the orientation of the white matter fibers is not continuous with that in the gray matter. The yellow arrow indicates a region of very low FA. (*E–H*) Myelin-stained sections corresponding to the subregions of the brain shown in *A–D*. (*E*) Coronal slice of the region in *A* showing the darkest staining within the white matter. (*F*) The *Inset* in *E*, matching *B*. The dashed line corresponds to the approximate correct position of the IPL convexity, compensating for a mounting artifact with this histological slice. The blue contour estimates the WGB based on a discontinuity in staining intensity. (*G*) Magnified view of the myelin fibers radiating into the IPL (white arrow), appearing to match the DTI orientations seen in *C*. (*H*) Magnified view of the sulcus myelin pattern, showing a lack of radial penetrations as well as matted fibers (yellow arrow) in the position of the low FA shown in *D*.

largely parallel to the gray matter diffusion orientations. In contrast, the principal fiber orientation in the magnified red region, from the adjacent fundus of the IPS, is nearly parallel to the WGB and hence is perpendicular to the overlying cortex. The myelin-stained sections in Fig. 1 *E–H* highlight fiber features that contribute to the measured diffusion orientation and FA information, including the matted pattern of myelinated fibers in the cortex of the sulcus that gives rise to the regions of particularly low FA (yellow arrow). Such matted fibers have been observed previously in the vicinity of sulci (38, 41, 42). Given these profound differences in local diffusion orientation, we next investigated the ability of dMRI tractography to identify pathways from the cortex into the deep white matter.

Seeding the Gray Matter: Biased Penetration into Deep White Matter. Long-range cortical connections involve axons from a given cortical position passing through the superficial white matter into the deep white matter and then on to a distant cortical or subcortical structure. The accurate detection of such connections using tractography requires that projections can be followed in contiguous voxels based on the local diffusion profile measured at each position. Capitalizing on the reliable diffusion orientation in the gray matter voxels of the present datasets, we were able to initiate tracking using pure gray matter seeds. We initiated gray matter seeding from the cortical midthickness because it minimized the chances of partial volume effects associated with the WGB boundary. With such seeding we found that throughout the cortex track lines emanating from such seeds successfully crossed the WGB, exiting the gray matter into the white matter. However, we found that despite the reliable entry of track lines into the superficial white matter, the subsequent fate of individual tracking attempts was strongly determined by the structure of the local fiber system. Specifically, track lines frequently became trapped within particular types of superficial white matter and thus failed to reach the deep white matter or distant cortical targets. This observation is exemplified in four seeds from the dorsal motor cortex and IPS (Fig. 2), which were representative of sulcal and gyral locations in many other regions of the cortex. Although previous macaque anatomical studies have shown that each of these cortical positions gives rise to long-range axonal projections (9, 28, 43–47), we found that the resulting track lines in most cases failed to escape the local white matter environment. In fact, of the four seeds shown in this example only seed 2, on the precentral gyrus, extended beyond the superficial association fibers and into the deeper white matter. In the brain of a second animal, the same gray matter seeds showed similar regional differences in their track line patterns, again with only seed 2 showing some deep white matter labeling (Fig. S3).

We next investigated the extent to which superficial white matter systems impede long-range tractography across the entire cortical surface. To examine this question systematically, we devised a simple measure, called the "voxel intersection count" (VIC), to assess the tracking from a gray matter seed. The VIC is a computed value that is proportional to the total number of voxels reached by track lines seeded from a given cortical position,

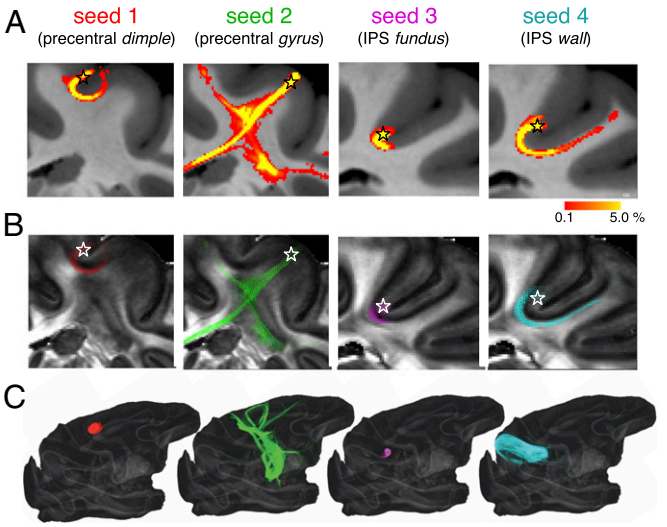

Fig. 2. Gray-matter seeding from two pairs of nearby positions, demonstrating that the precise positioning of gray matter seeds impacts the success of tracking into the deep white matter. (*A*) FSL track line density derived from four different seeds. Seeds 1 and 2 are less than 2 mm apart in the dorsal motor region, and seeds 3 and 4 are less than 1 mm apart in the IPS. In each case, 10,000 probabilistic track lines were seeded from a single surface coordinate within the middle thickness of the gray matter. The color map indicates the percentage of the track lines that reached a given voxel. Despite the physical proximity and, in the case of seeds 1 and 2, the functional and cytoarchitectural similarity of the seed regions, the track lines emanating from the four example seed locations varied markedly in their white matter penetration. Track lines emanating from seeds 1, 3, and 4 became trapped in local fiber systems and failed to enter the deep white matter. Probability tracks were overlaid on MTR maps. (*B*) Tracks from each seed in *A*, shown as the dominant orientation in each voxel reached by probabilistic tracking, overlaid on FA maps. (*C*) The 3D maps of the entire brain show the tracking of distance projections for each of the seeds.

expressed in parts per million (ppm). For example, if a hemisphere consists of a total of 2 million voxels, then a VIC of 100 ppm would indicate that the average track line from a seed position intersected with 200 voxels. Thus, the VIC from each cortical seed position served as surrogate for estimating deep white matter penetrance. Computing this value from all positions (nodes) on the extracted cortical surface provided a complete cortical map of deep white matter penetrance (Fig. 3*A*). The relationship between a VIC value and the distribution of track lines can be seen for the four previous example seeds (Fig. 3 *B* and *C*; see also Fig. 2). Track lines from seeds 1 and 3 reached only the local fiber systems and therefore had relatively low VIC values (36.8 and 23.2 ppm, respectively). Seed 2, despite being separated from seed 1 by less than 2 mm, had considerable deep white penetration resulting in a higher VIC value (143.9 ppm). Seed 4, situated less than 2 mm from seed 3, was intermediate in its track line penetrance, reaching some neighborhood fibers (39) but failing to connect with long-distance fiber tracts (VIC value, 75.6 ppm). Mapping the VIC over the cortical surface revealed a mosaic pattern of high and low VIC values, with the highest values typically associated with gyri and the lowest values in and around sulci. Less than half the cortex showed VIC values that suggested significant penetration into the deep white matter. We

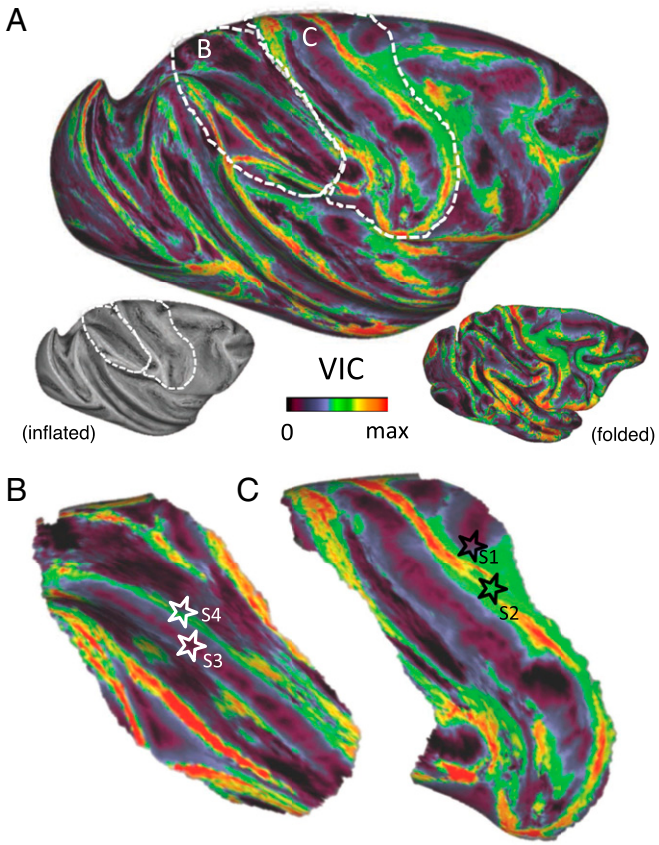

Fig. 3. (*A*) Map of VIC from the gray matter of an entire cerebral hemisphere. The VIC is a normalized measure of the number of voxels reached by the track lines from a given gray matter seed. As such, it indicates the success of tractography from a given cortical position in forming long tracks. Each cortical surface node was seeded 200 times, and the number of voxel-intersection events was recorded. The VIC index reflects both the number of voxels that were reached and how often they were reached over multiple instantiations of the probabilistic tractography (*Methods*). (*B*) The IPS region, including the positions of seeds 3 and 4 from Fig. 2 (white stars), seeded 1,000 times. (*C*) Central sulcus region, including the positions of seeds 1 and 2 from Fig. 2 (black stars), seeded 1,000 times.

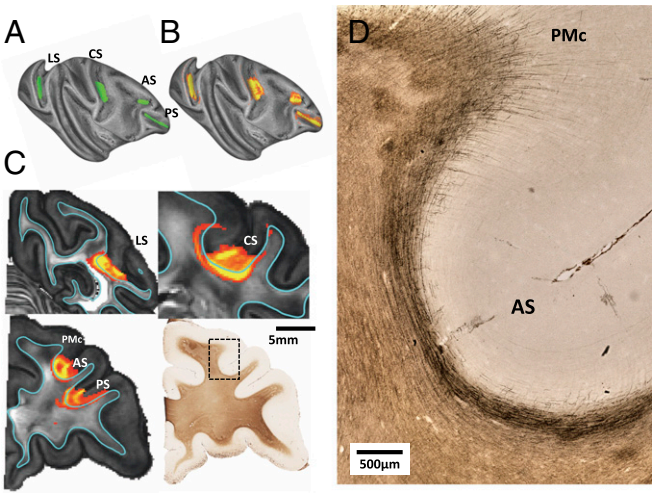

Fig. 4. Examples of broader gray matter seeding in sulci. Despite the larger seeding regions, the track lines are restricted by the dense U-fiber bundles in the superficial white matter. (*A*) Larger seed regions in four prominent sulci. (*B*) Track lines from these seed regions remain restricted to the local sulcus environment and fail to produce labeling elsewhere in the cerebral cortex despite the known long-range projections. (*C*) Visualization of the white matter distribution of the track line spreading for each seed in *A*, together with myelin-stained histological slide corresponding to two of the seeds. (*D*) Magnified view of myelin-stained histological section in the vicinity of the arcuate sulcus featured in the histological section in *C*. Stained fibers surrounding the sulcus are generally parallel to the WGB, whereas those at the adjacent gyrus are primarily radial in their orientation. This difference is presumed to give rise to the gyral bias associated with gray matter seeding. AS, arcuate sulcus; CS, central sulcus; LS, lateral sulcus; PMc, caudal premotor; PS principal sulcus.

determined this value by considering seed 4 in Fig. 2 as a conservative threshold for deep white matter penetration, categorizing those cortical sites with higher VIC values as exhibiting successful deep white matter penetrance. We found that 76% of cortical nodes had VIC values that were no larger than that of seed 4, suggesting that no more than 24% of seeds along the cortex could be said to reach deep white matter systems. Thus, according to this criterion, more than three quarters of cortical sites were ineligible for long-range tractography using a pure cortical seed. The overall magnitude and general pattern of the VIC maps computed from the brains of the two different monkeys showed good correspondence (Fig. S4*A*).

The effect of using larger cortical seeds is shown in Fig. 4 *A* and *B*. In this case we asked whether the spatial pooling of low-VIC voxels in fundus regions might improve penetration into the deep white matter. The results plainly show that under these conditions the track lines remain restricted to the local environment. Given that long-range corticocortical projections involve both the sulcal and gyral regions (38, 48, 49), the extremely low VIC values observed over much of the cortex can be reasonably interpreted as a failure of the dMRI tractography. Inspection confirmed that this failure is not caused by either the low FA of the cortex or the inability to track across the WGB but instead results from the difficulty in negotiating the superficial white matter systems to reach the deeper white matter.

Comparing the penetrance of gray matter seeding to myelin-stained histological sections from the same brains allowed the visualization of superficial fiber features that likely determine the success of dMRI tracking. For example, two very different types of superficial white matter fibers are visible in and around the arcuate sulcus (Fig. 4 *C* and *D*). Surrounding the fundus of the arcuate sulcus is a dense bundle of axons, sometimes called "U-fibers," which is visible on the histological section. U-fibers

are associational projections and are known to connect proximate cortical regions, such as adjacent gyri (39). This fiber bundle is the source of the orientation signal parallel to the WGB that dominates the superficial white matter and traps the track lines from the cortical seeds. On the adjacent gyrus of the caudal premotor cortex (PMc), the white matter fiber geometry, and its relationship to the overlying cortex is very different. In the PMc, the radial fibers are clearly visible on the myelin-stained section and penetrate into the cortex itself. The diffusion track lines from this region were much further reaching and led to much more extensive penetration of the white matter, as can be seen by the high VIC values in Fig. 3. Throughout the cortex, most regions of successful diffusion track line penetration beyond the superficial fiber systems were located on gyral surfaces.

To visualize directly the course of fibers stemming from neurons in one such sulcal region, we performed an injection of the anterograde tracer biotinylated dextran amine (BDA) into the IPS of one monkey, in approximately the position of seed 3 shown in Figs. 2 and 3. As can be seen in Fig. 5, this injection resulted in the labeling of projection fibers that traversed the superficial white matter directly and entered the deep white matter. The very low VIC from the corresponding region of the IPS in Figs. 2 and 3 suggests that these traversing fibers escape detection of the probabilistic tractography.

We further discovered that, in addition to sulci, many gyral locations also contained local white matter systems that presented barriers for long-range tractography. An example of such a system can be seen in Fig. 6, which shows the obstacle posed by the complex arrangement of superficial white matter running along the gyral crown of the IPL. Similar to the case with sulci, Fig. 6*B* shows that a gray matter seed placed on this gyral region led to track lines that spread lengthwise along the gyral crest but did not enter the deep white matter and thus did not lead to labeling beyond the local fiber environment. Analysis of fiber orientation in both the dMRI data (Fig. 6*C*; see also Figs. S5 and S6) and the myelin-stained section (Fig. 6*D*) revealed that this poor penetration could be ascribed to an enclosed compartment of longitudinal fibers, which we term "crown fibers," running parallel to the WGB (white arrows in Fig. 6 *C* and *D*). These fibers were separated from a perpendicular set of radial fibers connecting to the deeper white matter (black arrows). These complex fiber system properties are reflected in locally heterogeneous VIC values along the IPL (Fig. 6*E*), with regions of low white matter penetration on the crown directly adjacent to regions of relatively high penetration on the ridge. The orientation of the crown fibers is examined further on three orthogonal sections using the directionally encoded color (DEC) maps in Fig. S5. Similar crown fiber systems were observed throughout multiple gyri in the brain.

In summary, gray matter seeding led to the identification of long-range connections over a very limited region of the cortex. The absence of connections in sulcal and certain gyral regions reflect tractography challenges associated with penetrating the superficial white matter systems rather than an absence of true anatomical connections.

Seeding the White Matter: Cortical Distribution Similar to Gray-Matter Seeding. In a complementary analysis, we next characterized the pattern of track lines entering the cortex following the extensive seeding of the white matter (Fig. 7). The approach is similar to that of a previous dMRI tractography investigation in which the entire white matter was seeded and cortical afferents were detected predominantly on cortical gyri (38). In that case, the authors attributed the limited sulcal terminations to the difficulty posed by sharp fiber curvature for tractography algorithms that, by convention, follow the lowest possible angular differences between adjacent voxels (50). Here we took a somewhat different approach that allowed us to investigate the contribution of local

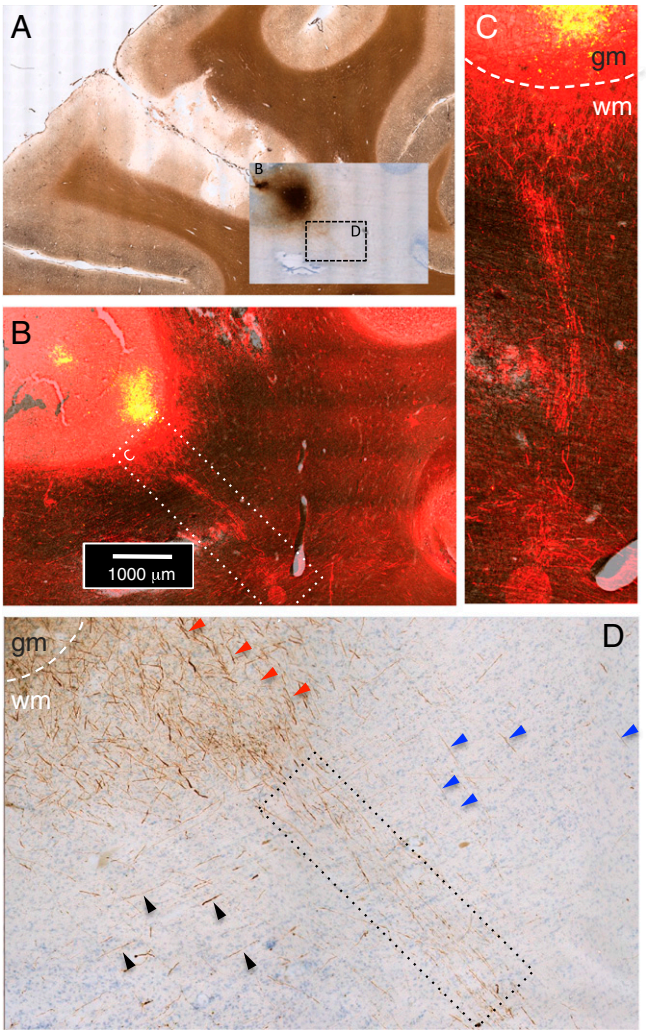

Fig. 5. Results of anatomical injection of BDA, an anterograde tracer, into the IPS. (*A*) View of the BDA injection site at the fundus of the IPS. (*Inset*) BDA staining on Nissl section, shown superimposed on a myelin-stained background. (*B*) Magnified view of the fundus depicting fluorescently immunolabeled BDA superimposed on a myelin-stained background. The dotted rectangle highlights a group of labeled fibers projecting from the fundus to deep white matter, crossing the superficial white matter. (*C*) Magnified view of the area within the dotted rectangle in *B*. The white dashed line indicates the WGB. (*D*) BDA-labeled white matter fibers from IPS fundus injection, magnified from the *Inset* in *A*. A group of labeled fibers (red arrowheads) projects radially through the superficial white matter into the deep white matter (dotted black rectangle). Sparse fibers oriented parallel (blue arrowheads) and perpendicular (black arrowheads) to the penetrating fiber group are visible also.

fiber systems. Rather than massively seeding the entire white matter, we seeded a large cross-section of the white matter near the midline. This noncortical seed region consisted of surface nodes on the medial aspect of the hemisphere that included the corpus callosum and internal capsule as well as midline subcortical gray matter. Each surface node was seeded 1,000 times. This method allowed us to follow long-range track lines originating in the large median seed and to examine the factors affecting tracking success, for example, in the transition from the deep to superficial white matter systems. The result of this seeding strategy was a map of midthickness gray matter penetration (Fig. 7*A*) that in many ways resembled both that found in the previous complete white matter seeding study (38) and the VIC map derived from gray matter seeding shown above (Fig. 3 and Fig. S4). As before, the most obvious feature was

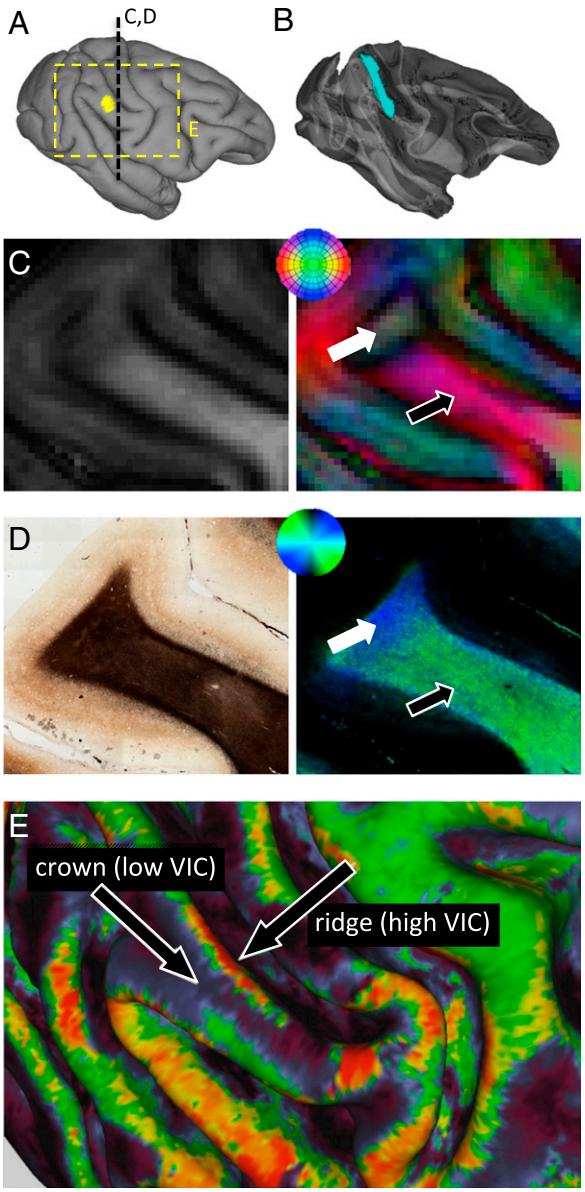

Fig. 6. Example of gyral region in which tracking is restricted by crown fibers. (*A*) The yellow area indicates the location of the seed in the ventral IPL, and the dashed line indicates the location of the histology sections shown in *C* and *D*. (*B*) Track lines emanating from the gyral seed are trapped within the local environment, in this case running along the gyral crown. (*C*) FA (*Left*) and DEC (*Right*) maps of the boxed region in *A* illustrate a clear directional compartmentalization, reflecting the dense bundle of longitudinal fibers running along the gyral crown. Although track lines propagate along the gyrus (white arrow), none can be observed entering the deeper white matter (black arrow), similar to the effects of U-fibers in fundus regions. (*D*) Histological section of tissue from the area mapped in *C* reveals similar compartmentalization of the white matter. Although the myelin-stained section (*Left*) reveals a largely uniform appearance of white matter at the crown, analysis of fiber orientation shows that the fibers in the crown do not have the same radial orientation as the deeper fibers, similar to the DEC map (*Right*). Orientation analysis used the principal eigenvector of the four-element structure tensor (*SI Methods*). Black and white arrows indicate the same orientation compartments shown in *C*. (*E*) VIC map showing the heterogeneous penetration of track lines from gray matter positions along a gyrus, in this case the IPL. Although the VIC values along the gyral ridges are relatively high, indicating that those regions can participate in long-range cortical connections, those along the gyral crown are much lower, reflecting the barrier posed by the longitudinal crown fiber system.

a bias toward certain gyral crowns and against most sulcal regions. The white matter seed region is depicted by the yellow region on the right of Fig. 7*A*. In Fig. 7 *A* and *B*, there is no threshold in the probabilistic mapping. Thus, the absence of any color indicates that not a single fiber from the probabilistic seeding of the large white matter region ever led to a track line in that region. Strikingly, we found that 47% of the cortex was never penetrated by track lines emanating from the massive medial seed. In Fig. 7 *C* and *D*, we applied a low-value threshold of 10 track lines, which further exposed swaths of the cortex as well as certain white matter zones in which track line presentation was extremely sparse or absent. For example, Fig. 7*D* is a magnified region of the central sulcus for which few or no track lines enter the superficial white matter zone, thus explaining why connections are absent in the overlying cortical region. These results show that, as with the gray matter seeding approach, only about half of cortical sites were eligible for long-range tracking. Although, as suggested previously (38), the sharp curvature of axons entering and exiting the cortex may contribute significantly to the gyral tractography bias, our analysis suggests that the dense local fiber subsystems pose an additional, and perhaps more daunting, challenge.

Impact of Seeding Strategy and Spatial Resolution. We next returned to gray matter seeding and asked how different types of seeding affect white matter penetration. A related variable that we also investigated was spatial resolution, because the effective size of voxels affects the blending of gray and white matter in and around the WGB. We focused on seeding in the vicinity of a sulcus, where we demonstrated that such tracking is most problematic (Figs. 2–4).

We found that white matter penetration was strongly affected by the strategy used for gray matter seeding as well as by the effective spatial resolution of the dMRI data. In both cases, the critical factor was whether the seed included portions of the white matter. As described above, we showed that pure gray matter seeding of the IPS did not escape the local environment (see seed 3 in Fig. 2). A similar result was obtained if we broadened this seed within the cortex, to include a slab of gray matter centered on the middle of the cortex (Fig. 8*A*). However, when an equivalent slab was simply translated deeper to a lower laminar position, now straddling the WGB, the track lines were notably more widespread (Fig. 8*B*). Tracks from this type of seed ran along the walls of the sulcus to the ridges of the IPL and postcentral gyrus, two regions with elevated VIC in Fig. 3, as well as to deeper regions of the white matter that led to cortical labeling some more distant regions, such as the precentral gyrus. Importantly, although the track lines apparently were more successful in escaping the local superficial white matter systems, this broader projection pattern is unlikely to reflect an accurate portrait of anatomical targets from that fundus region. Indeed, anatomical tracing studies investigating projections from this seed region (47) suggest that the tractography results from Fig. 8*B* have little to do with the actual distribution of anatomical projections. Our results suggest that the approach of expanding gray matter seeds to incorporate nearby voxels in the white matter is prone to serious error, because track lines will incorrectly enter white matter systems that are passing through the superficial white matter but have no direct relationship to the overlying cortex.

As a final experiment, we resampled the high-resolution data to a lower resolution (1 mm isotropic) to approximate the resolution that now is feasible for human dMRI tractography studies and soon may be commonplace. When the cortical midthickness seeding approach was applied to these data, but now with the larger voxels, there was incursion of the seed into the white matter, and we found that the computed track lines were even more widespread (Fig. 8*C*). The abundance of penetrating track lines at

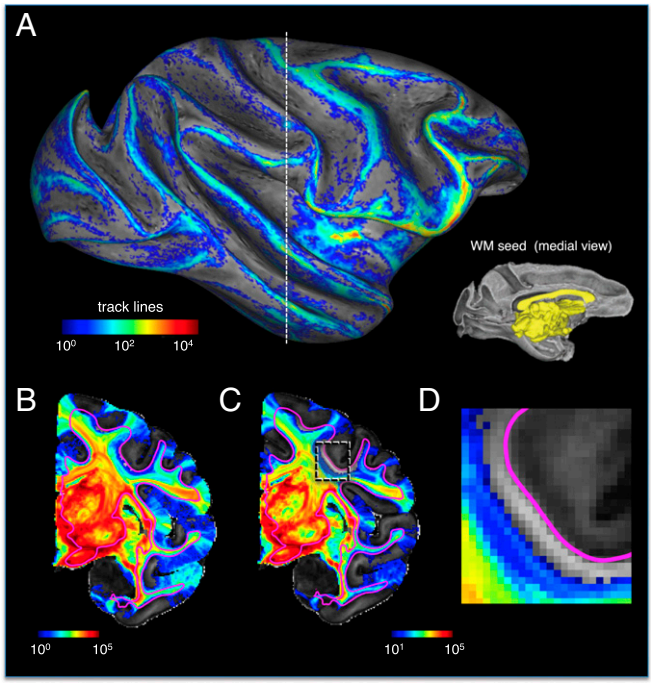

Fig. 7. Penetration of track lines into the cortex following white matter seeding. (*A*) Cortical labeling of track line penetration following massive a white matter seed that includes the internal capsule and corpus callosum (yellow region in *Inset*). (*B*) Seeding resulted in a massive spread of track lines across the hemisphere but in a rather limited and heterogeneous penetration into the gray matter. In this figure, there is no threshold in the probabilistic tracking; thus areas without color did not receive a single track line following the massive white matter seed. (*C*) As in *B* but with a threshold of 10 track lines, allowing visualization of a large portion of the cerebral cortex for which long-range tracking is almost nonexistent. (*D*) Magnification of a portion of the central sulcus with the same threshold as in *C*. This region of white matter, ~1 mm wide, running just below the WGB, along with the overlying cortex, is devoid of any afferent track lines. Together, this analysis shows that even with massive white matter seeding, significant portions of the gray matter do not register long-range connections.

low resolution can be understood by the combination of heterogeneous fibers within single voxels, resulting in the probabilistic tractography drawing from a broader distribution of orientations from each voxel. This mixture offers more opportunities for continuous tracking, overcoming sharp barriers such as the narrow band of U-fibers below the WGB. It must be emphasized, however, that this apparent success in escaping the local fiber environment does not indicate that the lower-resolution acquisition can track long-range cortical projections accurately. Instead, the low-resolution sampling gains its penetration into the white matter by decreasing, rather than increasing, the degree to which tracking reflects true anatomical connectivity. In essence, the lower resolution leads to a higher diffusive saturation of the white matter that falls off with the distance from the seed but has little anatomical specificity.

Discussion

The Challenges of Superficial White Matter. dMRI is unique in its capacity to investigate fiber systems and other structural features noninvasively in the living human brain. It is of great value to both researchers and clinicians. The present study focused on one aspect of dMRI analysis, namely the role of superficial white matter systems (i.e., subcortical white matter immediately underneath the deepest cortical layer) in limiting the tracking of long-range anatomical fibers to and from the cerebral cortex. Using high-quality ex vivo scans of the monkey brain at high resolution, we found that superficial white matter systems pose impediments for crossing into and out of the cortical surface over more than half of the cortical hemisphere.

By creating two types of cortical connectivity maps, we separately investigated the impact of these barriers on fiber traceability with both gray matter and white matter seeding approaches. The results from both approaches led to the disconcerting conclusion that only a relatively small proportion of the cerebral cortex is able exchange any track lines with the deep white matter. In general, in agreement with previous observations (36–38), seeding was more successful on gyral crowns than in sulci. Our findings suggest that this bias results in large measure from the challenges for tractography posed by superficial white matter systems. At present, the true trajectory of fibers passing from the more problematic gray matter regions is poorly characterized across the cerebral cortex, although our anterograde tracer injection demonstrates that fibers directly traverse the superficial white matter in at least some areas. If deep-going projections cross the local U-fiber systems perpendicularly, the failure to detect them may stem from the concentration of local diffusion energy in the principal direction of the U-fibers. Moreover, to the extent that deep-going projections join the U-fibers temporarily, run parallel to the WGB for a period, and then dive toward the deep matter, detecting such connections may be even more difficult. Importantly, tracer injections in the monkey indicate no particular bias of superficial white matter projections arising in gyri rather than sulci (ref. 38, and see supplemental data in ref. 48). Although it may be unwise to assume that the exchange of projections with the deep white matter is uniform in its density across the cortex, changes in projection density alone cannot account for our findings. Our anterograde tracer injection experiment (Fig. 5) further revealed not only that real long-range projections penetrate the

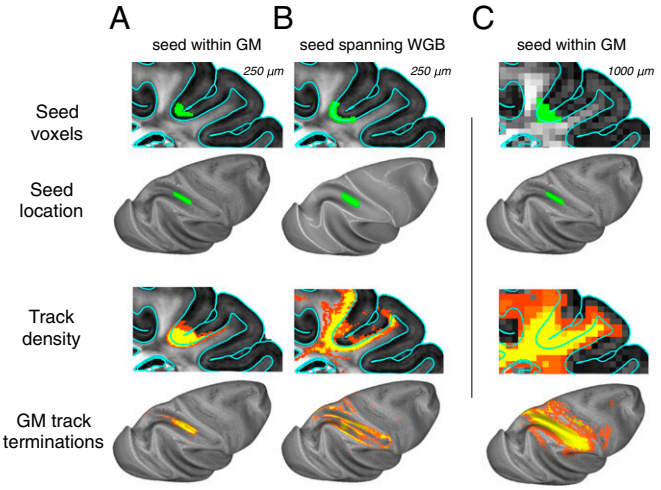

Fig. 8. Effect of gray matter seeding strategy and spatial resolution on penetration of track lines into the deep white matter. The upper two rows show seeding strategy, and the lower two rows show distribution of track lines. (*A*) A slab of voxels (rather than surface coordinates used elsewhere in this study) was used to create a tractography seed region in the fundus of the IPS. Voxels were selected within a region projected 250 μm above and below the cortical midthickness. Examination of the resulting track density and track termination plots revealed that this large seed led to minimal labeling away from the IPS, consistent with the results shown in Fig. 2. (*B*) Shifting an equivalent slab to straddle the WGB led to more widespread labeling, particularly on adjacent gyri. (*C*) In a 1-mm isotropic dMRI dataset, down-sampled from the 250-μm dataset, voxels projected using 250-um methods and parameters identical to those used in *A* resulted in an even broader spread of track lines. Note that the increased spatial distribution in *B* and *C* did not improve the accuracy of projections emanating from the overlying cortex but simply reflected the seeding of superficial, broadly projecting white matter tracts.

superficial white matter system but also that the bundling of projection fibers can vary widely even from a single injection site. Establishing the ground truth on such matters through anatomical tracer experiments may be the only way forward to optimize algorithms to reflect true anatomical connectivity maximally.

The most successful tractography penetration to and from the white matter occurred for voxels on gyral surfaces. This success may result in part from geometrical reasons, because the diffusion orientations of fibers entering gyri are well aligned to penetrate straight into the crown. However, our observations suggest that a more important reason for the gyral bias may rest on the organization of superficial fibers. Dense associational fiber systems are prevalent in the superficial white matter of sulci but are less common in gyri. We found that in the cases where complex white matter fiber systems (crown fibers) do exist in crowns (Fig. 6), the overlying cortex was devoid of long-range connections in a manner that closely resembled the situation at the fundus of a sulcus. Although U-fibers are associated with the fundus and banks of a sulcus, crown fibers are associated with a convex surface. In both cases, superficial fiber systems dominate the local diffusion measurement and thus prevent the detection of corticocortical connections.

Implications for Current Tractography Practices. In the introduction we mentioned two practical means by which researchers presently combat the challenges associated with cortical diffusion tractography. The first is the inclusion of adjacent white matter voxels into a gray matter seed. It is easy to understand that, in cases where gray matter seeding is unsuccessful, such an extension of the seed region will lead to track lines entering the white matter (as shown in Fig. 8). However, our study demonstrates that track lines emanating from the white matter directly adjacent to a given cortical position are unacceptable as surrogates for the fibers entering and leaving that cortical region. In fact, the results suggest that for at least half of the cortex the main orientation of the diffusion displacement profile in these white matter voxels is discordant with that found in the overlying cortex (see Figs. S7–S9), and thus expansion of seeds into the white matter could lead to incorrect tracking results (see Fig. 8*B* for an example). Seeding approaches more sophisticated than shifting a seed region into adjacent white matter may be developed in the future and might recognize and model the macroscopic diffusion fields over many neighboring voxels to facilitate track line passage through the superficial white matter fiber systems. The second practice of using waypoints to include only tracts that are explicitly in the desired position is questionable, in that it implicitly assumes that diffusion tractography is little more than a visualization tool, lacking in intrinsic anatomical accuracy. There is an inherent trade-off in the detection of fiber tracts that can be negotiated by changing the tractography parameter settings: Liberal parameter settings that are sensitive to more subtle connections necessarily increase the detection of false connections, whereas conservative settings that minimize incorrect detections will miss more true connections (35). However, our findings demonstrate that some biases affecting cortical tractography are fundamental and cannot be overcome by the adjustment of parameters and the selection of waypoints. In that sense, they are consistent with and provide a mechanistic understanding for recent empirical work showing that even advanced tractography methods are unable to achieve simultaneously both high sensitivity and high specificity in the identification of cortical connections (35).

Although it is possible that still higher resolution and signal-to-noise acquisition will help track these currently undetectable projections, the present results suggest that this problem is likely to be an obstacle for dMRI tractography in the human brain for some time. The common approach of expanding the gray matter seed into the white matter is not a satisfactory solution to this problem, because there is no theoretical or empirical basis for expecting that the white matter portions of the seed are those that connect to the overlying gray matter. Instead, overcoming these challenges may hinge on the development of "smarter" tractography algorithms (51), in which the construction of track lines is based not only on the adjunction of neighboring voxels with similar diffusion orientation but also upon the wider characteristics of the local fiber environment. In addition, advanced methods to model fiber orientation more realistically in a MRI voxel, such as fanning models (52) may play an increasingly important role. It is worth noting that although much of the superficial white matter may be dedicated to local connections, "superficial" does not necessarily mean "local." A substantial proportion of the superficial white matter may send connections beyond the local neighborhood. For example, the longitudinal crown fibers may represent axonal connections between cortical areas separated by more than a centimeter. It remains to be seen whether moving away from purely data-driven tractography and allowing prior anatomical knowledge about superficial fibers systems to shape the way in which dMRI data are modeled will ultimately lead to more accurate identification of anatomical connections in the brains of humans and nonhuman primates. Any such advances will depend critically upon understanding the neuroanatomical structure of superficial white matter systems, the manner in which they are crossed by corticofugal and corticopetal fibers, and any principles upon which tracking algorithms might be modified to compensate for what now is an effective barrier to accurate tractography.

Methods

Brain Specimens and ex Vivo dMRI Data Acquisition. The brains of three healthy adult male macaque monkeys were included in this study. Two monkeys, case A (5.95 kg, 4.5 y old) and case B (5.3 kg, 7.8 y old), were used for the dMRI studies, and a third monkey was used for anatomical tracer injections. All procedures followed the Institute of Laboratory Animal Research (part of the National Research Council of the National Academy of Sciences) guidelines and were carried out under an animal study protocol approved by the National Institute of Mental Health Animal Care and Use Committee. The brains for dMRI were treated with gadopentetic acid (Gd-DTPA) (Magnevist; Berlex Laboratories) to reduce the longitudinal relaxation time (T1), immersed in Fomblin (Solvay Solexis Inc., West Deptford, NJ) to match the brain susceptibility, and sealed in a 60-mm-diameter Plexiglas tube (53, 54). Scanning was performed using a 30-cm 7-Tesla scanner (Bruker). The diffusion data were acquired with a standard spin-echo diffusion-weighted echo planar imaging (EPI) sequence (DtiEpi) available in Bruker Paravision software. The 3D dMRI image had an isotropic spatial resolution of 250 μm, with slightly different matrix sizes in the two animals (278 × 256 × 238 for case A; 256 × 296 × 256 for case B). Scanning sessions for acquisition of diffusion data for case A lasted approximately 3 d. Anatomical scans for magnetization transfer ratio (MTR) contrast (55) scans served as a measure of gray/white contrast. Following dMRI data collection over approximately 5 mo, the brain of case A was prepared for histological sectioning and Gallyas myelin staining and analysis of axonal fibers.

MRI Data Analysis. The dMRI data were preprocessed using TORTOISE software package (56) and reoriented to be approximately parallel to the anterior commissure–posterior commissure (ACPC) line. Models of the WGB and pial surfaces were computed using the MTR images with FreeSurfer software (surfer.nmr.mgh.harvard.edu) (57). Probabilistic modeling and tractography was performed using FMRIB Software Library (FSL) 5.1 (fsl.fmrib.ox.ac.uk/fsldownloads). Surface nodes, serving as positional coordinates along the cortical midthickness, then were used as seeds initiating for track lines, whose distribution throughout the cerebral hemisphere was of principal interest. All data were imported into the Connectome Workbench software (www.humanconnectome.org/software) for analysis and visualization (58). To evaluate the penetrance of gray matter seeding over the cortical surface, we computed the voxel VIC, corresponding to a normalized measure of track line distribution throughout the hemisphere from each position. This measure, expressed in parts per million, indicates the overall density of labeling throughout the entire brain from a given seed location. Because larger values indicate a wider distribution of track lines, this measure serves as a surrogate for white matter penetration. To evaluate further long-range fiber penetration in the cortex, we measured track lines in the cortical gray matter stemming from a massive white matter seed on the medial surface of the brain that encapsulated the corpus callosum and the internal capsule.

ACKNOWLEDGMENTS. We thank Dr. Cibu Thomas for critical comments on the manuscript and Drs. Donna Dierker, Tim Coalson, and Matt Glasser for advice and discussion, and Drs. Hellmut Merkle, Daniel Papoti, and Charles Zhu for technical assistance. This work was supported by the Intramural Research Programs of the National Institute of Mental Health, National Institute of Neurological Disorders and Stroke, and the National Eye Institute. C.R. and A.K.S. received support from the School of Informatics at the University of Sussex and the Dr. Mortimer and Theresa Sackler Foundation.

1. Zilles K, Amunts K (2010) Centenary of Brodmann's map—conception and fate. *Nat Rev Neurosci* 11(2):139–145.
2. Tootell RB, Hadjikhani NK, Mendola JD, Marrett S, Dale AM (1998) From retinotopy to recognition: fMRI in human visual cortex. *Trends Cogn Sci* 2(5):174–183.
3. Op de Beeck HP, Haushofer J, Kanwisher NG (2008) Interpreting fMRI data: Maps, modules and dimensions. *Nat Rev Neurosci* 9(2):123–135.
4. Smith SM, et al. (2013) Functional connectomics from resting-state fMRI. *Trends Cogn Sci* 17(12):666–682.
5. Sporns O (2013) The human connectome: Origins and challenges. *Neuroimage* 80: 53–61.
6. Kaas JH (2012) The evolution of neocortex in primates. *Prog Brain Res* 195:91–102.
7. Mantini D, et al. (2012) Interspecies activity correlations reveal functional correspondence between monkey and human brain areas. *Nat Methods* 9(3):277–282.
8. Tsao DY, Moeller S, Freiwald WA (2008) Comparing face patch systems in macaques and humans. *Proc Natl Acad Sci USA* 105(49):19514–19519.
9. Felleman DJ, Van Essen DC (1991) Distributed hierarchical processing in the primate cerebral cortex. *Cereb Cortex* 1(1):1–47.
10. Perelman P, et al. (2011) A molecular phylogeny of living primates. *PLoS Genet* 7(3): e1001342.
11. Van Essen DC, Glasser MF, Dierker DL, Harwell J, Coalson T (2012) Parcellations and hemispheric asymmetries of human cerebral cortex analyzed on surface-based atlases. *Cereb Cortex* 22(10):2241–2262.
12. Crick F, Jones E (1993) Backwardness of human neuroanatomy. *Nature* 361(6408): 109–110.
13. Sporns O, Tononi G, Kötter R (2005) The human connectome: A structural description of the human brain. *PLOS Comput Biol* 1(4):e42.
14. Van Essen DC, Ugurbil K (2012) The future of the human connectome. *Neuroimage* 62(2):1299–1310.
15. Mufson EJ, Brady DR, Kordower JH (1990) Tracing neuronal connections in postmortem human hippocampal complex with the carbocyanine dye DiI. *Neurobiol Aging* 11(6):649–653.
16. Tardif E, Clarke S (2001) Intrinsic connectivity of human auditory areas: A tracing study with DiI. *Eur J Neurosci* 13(5):1045–1050.
17. Molnár Z, Blakey D, Bystron I, Carney RSE (2006) *Neuroanatomical Tract-Tracing 3*, eds Zaborszky L, Wouterlood FG, Lanciego JL, Heimer L (Springer, New York, NY), pp 366–393.
18. Seehaus AK, et al. (2013) Histological validation of DW-MRI tractography in human postmortem tissue. *Cereb Cortex* 23(2):442–450.
19. Van Essen DC, et al.; WU-Minn HCP Consortium (2012) The Human Connectome Project: A data acquisition perspective. *Neuroimage* 62(4):2222–2231.
20. Basser PJ, Mattiello J, LeBihan D (1994) MR diffusion tensor spectroscopy and imaging. *Biophys J* 66(1):259–267.
21. Pierpaoli C, Jezzard P, Basser PJ, Barnett A, Di Chiro G (1996) Diffusion tensor MR imaging of the human brain. *Radiology* 201(3):637–648.
22. Behrens TEJ, et al. (2003) Non-invasive mapping of connections between human thalamus and cortex using diffusion imaging. *Nat Neurosci* 6(7):750–757.
23. Mori S, van Zijl PCM (2002) Fiber tracking: Principles and strategies - a technical review. *NMR Biomed* 15(7-8):468–480.
24. Wedeen VJ, Hagmann P, Tseng W-YI, Reese TG, Weisskoff RM (2005) Mapping complex tissue architecture with diffusion spectrum magnetic resonance imaging. *ISMRM Proceedings* 54:1377–1386.
25. Wedeen VJ, et al. (2012) The geometric structure of the brain fiber pathways. *Science* 335(6076):1628–1634.
26. Catani M, Jones DK, Donato R, Ffytche DH (2003) Occipito-temporal connections in the human brain. *Brain* 126(Pt 9):2093–2107.
27. Jbabdi S, Behrens TEJ, Smith SM (2010) Crossing fibres in tract-based spatial statistics. *Neuroimage* 49(1):249–256.
28. Schmahmann JD, et al. (2007) Association fibre pathways of the brain: Parallel observations from diffusion spectrum imaging and autoradiography. *Brain* 130(Pt 3): 630–653.
29. Jbabdi S, Lehman JF, Haber SN, Behrens TE (2013) Human and monkey ventral prefrontal fibers use the same organizational principles to reach their targets: Tracing versus tractography. *J Neurosci* 33(7):3190–3201.
30. Dauguet J, et al. (2007) Comparison of fiber tracts derived from in-vivo DTI tractography with 3D histological neural tract tracer reconstruction on a macaque brain. *Neuroimage* 37(2):530–538.
31. Dyrby TB, et al. (2007) Validation of in vitro probabilistic tractography. *Neuroimage* 37(4):1267–1277.
32. Kleiser R, Staempfli P, Valavanis A, Boesiger P, Kollias S (2010) Impact of fMRI-guided advanced DTI fiber tracking techniques on their clinical applications in patients with brain tumors. *Neuroradiology* 52(1):37–46.
33. Kitamura K, et al. (2008) Diffusion tensor imaging of the cortico-ponto-cerebellar pathway in patients with adult-onset ataxic neurodegenerative disease. *Neuroradiology* 50(4):285–292.
34. Jbabdi S, Johansen-Berg H (2011) Tractography: Where do we go from here? *Brain Connect* 1(3):169–183.
35. Thomas C, et al. (2014) Anatomical accuracy of brain connections derived from diffusion MRI tractography is inherently limited. *Proc Natl Acad Sci USA* 111(46): 16574–16579.
36. Chen H, et al. (2013) Coevolution of gyral folding and structural connection patterns in primate brains. *Cereb Cortex* 23(5):1208–1217.
37. Nie J, et al. (2012) Axonal fiber terminations concentrate on gyri. *Cereb Cortex* 22(12): 2831–2839.
38. Van Essen DC, et al. (2013) *Diffusion MRI: From Quantitative Measurement to in Vivo Neuroanatomy* (Academic, Burlington, MA), p 2nd Ed, p 576.
39. Schmahmann JD, Pandya D (2009) *Fiber Pathways of the Brain* (Oxford Univ. Press, New York).
40. Gray H (1918) *Anatomy of the Human Body* (Lea and Febiger, Philadelphia).
41. Lewis JW, Van Essen DC (2000) Mapping of architectonic subdivisions in the macaque monkey, with emphasis on parieto-occipital cortex. *J Comp Neurol* 428(1):79–111.
42. Preuss TM, Goldman-Rakic PS (1991) Architectonics of the parietal and temporal association cortex in the strepsirhine primate Galago compared to the anthropoid primate Macaca. *J Comp Neurol* 310(4):475–506.
43. Gharbawie OA, Stepniewska I, Qi H, Kaas JH (2011) Multiple parietal-frontal pathways mediate grasping in macaque monkeys. *J Neurosci* 31(32):11660–11677.
44. Tokuno H, Takada M, Nambu A, Inase M (1997) Reevaluation of ipsilateral corticocortical inputs to the orofacial region of the primary motor cortex in the macaque monkey. *J Comp Neurol* 389(1):34–48.
45. Leichnetz GR (1986) Afferent and efferent connections of the dorsolateral precentral gyrus (area 4, hand/arm region) in the macaque monkey, with comparisons to area 8. *J Comp Neurol* 254(4):460–492.
46. Geyer S, Matelli M, Luppino G, Zilles K (2000) Functional neuroanatomy of the primate isocortical motor system. *Anat Embryol (Berl)* 202(6):443–474.
47. Lewis JW, Van Essen DC (2000) Corticocortical connections of visual, sensorimotor, and multimodal processing areas in the parietal lobe of the macaque monkey. *J Comp Neurol* 428(1):112–137.
48. Markov NT, et al. (2014) A weighted and directed interareal connectivity matrix for macaque cerebral cortex. *Cereb Cortex* 24(1):17–36.
49. Markov NT, et al. (2011) Weight consistency specifies regularities of macaque cortical networks. *Cereb Cortex* 21(6):1254–1272.
50. Behrens TEJ, Berg HJ, Jbabdi S, Rushworth MFS, Woolrich MW (2007) Probabilistic diffusion tractography with multiple fibre orientations: What can we gain? *Neuroimage* 34(1):144–155.
51. Rowe M, Zhang HG, Oxtoby N, Alexander DC (2013) Beyond crossing fibers: Tractography exploiting sub-voxel fibre dispersion and neighbourhood structure. *Inf Process Med Imaging* 23:402–413.
52. Sotiropoulos SN, Behrens TEJ, Jbabdi S (2012) Ball and rackets: Inferring fiber fanning from diffusion-weighted MRI. *Neuroimage* 60(2):1412–1425.
53. D'Arceuil HE, Westmoreland S, de Crespigny AJ (2007) An approach to high resolution diffusion tensor imaging in fixed primate brain. *Neuroimage* 35(2):553–565.
54. Wedeen VJ, et al. (2008) Diffusion spectrum magnetic resonance imaging (DSI) tractography of crossing fibers. *Neuroimage* 41(4):1267–1277.
55. Wolff SD, Balaban RS (1989) Magnetization transfer contrast (MTC) and tissue water proton relaxation in vivo. *ISMRM Proceedings* 10:135–144.
56. Pierpaoli C, et al. (2010) TORTOISE: An integrated software package for processing of diffusion MRI data. *ISMRM Proceedings* 18:1597.
57. Dale AM, Fischl B, Sereno MI (1999) Cortical surface-based analysis. I. Segmentation and surface reconstruction. *Neuroimage* 9(2):179–194.
58. Marcus DS, et al.; WU-Minn HCP Consortium (2013) Human Connectome Project informatics: Quality control, database services, and data visualization. *Neuroimage* 80: 202–219.